School of Natural Sciences and Mathematics
William B. Hanson Center for Space Sciences

Modeling Energetic Electron Nonlinear Wave-Particle Interactions with Electromagnetic Ion Cyclotron Waves

UT Dallas Author(s):

Liheng Zheng
Lunjin Chen
Hui Zhu

Citation:

Zheng, L., L. Chen, and H. Zhu. 2019. "Modeling Energetic Electron Nonlinear Wave-Particle Interactions with Electromagnetic Ion Cyclotron Waves." Journal of Geophysical Research: Space Physics 124(5): 3436-3453, doi: 10.1029/2018JA026156

JGR Space Physics

RESEARCH ARTICLE
10.1029/2018JA026156

Modeling Energetic Electron Nonlinear Wave-Particle Interactions With Electromagnetic Ion Cyclotron Waves

Liheng Zheng[1], **Lunjin Chen**[1], **and Hui Zhu**[1]

[1]William B. Hanson Center for Space Sciences, Department of Physics, University of Texas at Dallas, Richardson, TX, USA

Key Points:
- A method is developed for modeling PSD evolution under nonlinear EMIC wave-particle interaction
- Nonlinear transport does not significantly change loss rate as compared to quasi-linear theory
- Our simulations predict peculiar negative electron loss cone PSD slopes in strong EMIC wavefield

Correspondence to:
L. Zheng and L. Chen,
zhengliheng@gmail.com;
lunjin.chen@gmail.com

Citation:
Zheng, L., Chen, L., & Zhu, H. (2019). Modeling energetic electron nonlinear wave-particle interactions with electromagnetic ion cyclotron waves. *Journal of Geophysical Research: Space Physics*, *124*, 3436–3453. https://doi.org/10.1029/2018JA026156

Received 2 OCT 2018
Accepted 28 FEB 2019
Accepted article online 15 APR 2019
Published online 31 MAY 2019

Abstract Electromagnetic ion cyclotron (EMIC) waves in duskside plasmasphere and plasmaspheric plume scatter megaelectron volt electrons into the loss cone and are considered a major loss mechanism for the outer radiation belt. Wave-particle interaction between energetic electrons and EMIC waves has been studied extensively by the quasi-linear diffusion theory. However, EMIC waves are typically strong enough to trigger nonlinear wave-particle interaction effects and transport electrons in very different ways from quasi-linear diffusion. New mathematical method is therefore in demand to study the evolution of energetic electron distribution in response to nonlinear wave-particle interaction. In this work, we present a Markov chain description of the wave-particle interaction process, in which the electron distribution is represented by a state vector and is evolved by the Markov matrix. The Markov matrix is a matrix form of the electron response Green's function and could be determined from test particle simulations. Our modeling results suggest that electron loss rate is not significantly affected by phase bunching and phase trapping, but for strong EMIC waves, electron distribution is more saturated near loss cone than quasi-linear theory prediction, and negative electron phase space density slope develops inside loss cone.

1. Introduction

Electromagnetic ion cyclotron (EMIC) waves are naturally occurring emissions in the Earth's magnetosphere, often observed along the duskside plasmapause (Fraser et al., 1996) or in the plasmaspheric plumes (Anderson et al., 1992; Morley et al., 2009). These waves can be excited below the proton gyrofrequency via cyclotron resonance with anisotropic ring current protons (e.g., Horne & Thorne, 1993; Jordanova et al., 2001; Mauk & McPherron, 1980; Thorne & Horne, 1997), which are injected into plasmasphere and plume near the equatorial region during storm times (Chen et al., 2010; Jordanova et al., 2006). The EMIC wave frequency spectrum is typically separated into three bands below the hydrogen (H^+), helium (He^+), and oxygen (O^+) gyrofrequencies (Horne & Thorne, 1994; Kozyra et al., 1984). He^+ band EMIC waves are found to be statistically most intense during active conditions (Fraser et al., 2010) and can attain large wave numbers in the cold plasma limit, thus acting as a potential candidate for resonant scattering radiation belt electrons into atmosphere (Meredith et al., 2003; Shprits, 2009; Shprits et al., 2016; Thorne & Kennel, 1971). Quasi-linear diffusion theory (Kennel & Engelmann, 1966) has mostly been employed to model these wave-particle interactions (Jordanova et al., 2008; Lyons, 1974; Miyoshi et al., 2008; Summers & Thorne, 2003). However, typical strong EMIC wave intensities in the outer radiation belt (1–10 nT) raise doubt about the validity of the quasi-linear framework.

Wave-particle interaction goes into nonlinear regime when the waves are strong in amplitude and coherent in phase (Albert, 2000, 2002; Albert & Bortnik, 2009; Albert et al., 2013; Omura et al., 2008). These waves scatter electrons in a different way than would have been expected from quasi-linear theory. The large amplitude and phase coherence of these waves cause electrons to be phase bunched or phase trapped by the wavefield and hence to exhibit nondiffusive behaviors under resonance (Bortnik et al., 2008). Various test particle codes, based on either Newton-Lorentz equations (e.g., Chen et al., 2016; Omura & Summers, 2004; Tao & Bortnik, 2010) or Hamiltonian mechanics (e.g., Albert, 2000; Artemyev et al., 2016), have been developed to study the behavior of charged particles in strong and coherent wavefields. Test particle simulations show that nonlinear interaction with monochromatic EMIC waves can scatter electron pitch angles by tens of degrees on a time scale of a few seconds (Albert & Bortnik, 2009), whereas it would typically cost minutes

for quasi-linear diffusion to do so. Yet how radiation belt electron distributions respond to these nonlinear interactions with EMIC waves has remained an open question. In seeking for an answer, it is the purpose of this work to provide a method for modeling statistical behavior of radiation belt electrons under nonlinear interaction with EMIC waves.

2. Mathematical Background

The stochastic motion of a particle undergone resonant interaction with plasma waves is essentially a Markov process. That means the state of the particle at a future time $t + \Delta t$, which may be described by, say, an action integral I, only depends on the state of the particle at the current time t but not on the previous history. For simplicity of presentation, all equations in this section will be with respect to the canonical variable I; their forms are unchanged in other noncanonical coordinates, except for equations (6), (7), and (9), which would involve a Jacobian determinant. Appendix A gives mathematical derivations of the equations satisfied by a Markovian transition probability. From those results, for an ensemble of such particles with a distribution function $F(I, t)$, the Markovian property is fully expressed by the Chapman-Kolmogorov equation as

$$F(I, t + \Delta t) = \int \mathrm{d}I' P(I, \Delta t|I')F(I', t), \tag{1}$$

where $P(I, \Delta t|I')$ is the transition probability density from I' to I in Δt time: It serves the role as a Green's function of the process. Repeated convolution over the Green's function as that in equation (1) therefore gives a temporal evolution of the distribution function. Ignoring loss mechanisms, Furuya et al. (2008) and Omura et al. (2015) used this equation to calculate radiation belt electron distribution responses to nonlinear chorus wave emissions, wherein the Green's functions were numerically determined from test particle simulations over one resonance with chorus waves.

Following the details in Appendix A, time derivative of $F(I, t)$ can be straightforwardly derived from equation (1) and expressed by the master equation

$$\frac{\partial}{\partial t}F(I, t) = \int \mathrm{d}I' \left[Q(I|I')F(I', t) - Q(I'|I)F(I, t)\right], \tag{2}$$

in which $Q(I|I')$ is the transition rate from state I' to I, as defined by equation (A7). After integration, the first term on the right-hand side of equation (2) gives the number of particles entering an infinitesimal interval around I per infinitesimal time, and the second term gives the number of particles departing that state. If the stochastic changes are sufficiently small (see Appendix A for a precise definition), such as in the quasi-linear wave-particle interaction approximation, the right-hand side of equation (2) can be expanded into Kramers-Moyal series, which, by keeping the first two leading terms, yields the Fokker-Planck equation:

$$\frac{\partial}{\partial t}F(I, t) = -\frac{\partial}{\partial I}\left[B_I F(I, t)\right] + \frac{\partial^2}{\partial I^2}\left[D_{II}F(I, t)\right], \tag{3}$$

where the first and second transport coefficients are, respectively, evaluated by

$$B_I(I) = \lim_{\Delta t\to 0}\frac{1}{\Delta t}\int \mathrm{d}I'(I' - I)P(I', \Delta t|I), \tag{4}$$

$$D_{II}(I) = \lim_{\Delta t\to 0}\frac{1}{2\Delta t}\int \mathrm{d}I'(I' - I)^2 P(I', \Delta t|I). \tag{5}$$

Written in divergence form, the Fokker-Planck equation (3) becomes

$$\frac{\partial}{\partial t}F(I, t) = -\frac{\partial}{\partial I}\left[h_I F(I, t)\right] + \frac{\partial}{\partial I}\left[D_{II}\frac{\partial}{\partial I}F(I, t)\right], \tag{6}$$

where

$$h_I(I) = B_I(I) - \frac{d}{\mathrm{d}I}D_{II}(I). \tag{7}$$

From equation (6), we can identify that the first term on the right-hand side corresponds to an inward advection flux into a spatial element and the second term an inward diffusion flux. Therefore h_I, instead of B_I,

gives the correct advection coefficient: Besides the first transport coefficient B_I, it also takes into account the contribution from uneven distribution of the diffusion coefficient D_{II}. To distinguish, we henceforth call B_I the drift coefficient. In quasi-linear wave-particle interaction theory, no advection can be caused by stochastic scatterings; hence, h_I is identically 0 and equation (6) reduces to the familiar form of quasi-linear radiation belt Fokker-Planck equation (e.g., Schulz & Lanzerotti, 1974).

We note in passing that there has been some confusion in the literature in numerically evaluating the diffusion coefficient. In some works (e.g., Artemyev et al., 2017; Liu et al., 2010; Maldonado & Chen, 2018) the diffusion coefficient was calculated according to equation (5), whereas others (e.g., Artemyev et al., 2016; Chen et al., 2016; Su et al., 2012; Tao et al., 2011) essentially evaluated it using the statistical variation of I':

$$\begin{aligned} D^*_{II}(I) &\equiv \lim_{\Delta t\to 0}\frac{1}{2\Delta t}\left\langle \left(I'-\left\langle I'\right\rangle\right)^2\right\rangle \\ &= D_{II}(I)-\lim_{\Delta t\to 0}\frac{1}{2\Delta t}\left(\left\langle I'\right\rangle - I\right)^2, \end{aligned} \tag{8}$$

in which $\langle \dots \rangle = \int \mathrm{d}I' \dots P(I', \Delta t|I)$ stands for ensemble average. For small stochastic changes, D^*_{II} approaches D_{II} in the procedure $\Delta t \to 0$, since $(\langle I' \rangle - I)$ is proportional to Δt due to existence of the limit in equation (4). For large stochastic changes, the limits in equations (4) and (5) may not exist, and the concept of transport coefficients is quantitatively meaningless because the master equation (2) in this case cannot be approximated by a Fokker-Planck equation (see Appendix A).

A general nonlinear wave-particle interaction problem would require solving its distribution evolution by either equation (1) or (2) since the wavefield can be strong and so are the stochastic scatterings. However, if the wave is sufficiently weak, so that the particle potential energy in the wavefield is much smaller than its unperturbed Hamiltonian, the particle scatterings can be distinguished into transient resonances that are small in stochastic changes but possibly directional due to phase bunching and large stochastic jumps due to phase trapping (Artemyev et al., 2016, 2017; Artemyev, Neishtadt, Vainchtein, et al., 2018; Artemyev, Neishtadt, Vasiliev, et al., 2018). For megaelectron volt (MeV) electrons and whistler mode waves in the inner magnetosphere, this weak wave condition corresponds to a wave magnetic amplitude much less than 10 nT (Artemyev, Neishtadt, Vasiliev, et al., 2018). Then in the master equation (2), the transition rates corresponding to transient resonances can still be expanded into Kramers-Moyal series, and we are left with the following integro-differential kinetic equation

$$\begin{aligned} \frac{\partial}{\partial t}F(I,t) = &-\frac{\partial}{\partial I}\left[\tilde{h}_I F(I,t)\right]+\frac{\partial}{\partial I}\left[\tilde{D}_{II}\frac{\partial}{\partial I}F(I,t)\right] \\ &+\int \mathrm{d}I'\left[\mathcal{Q}(I|I')F(I',t)-\mathcal{Q}(I'|I)F(I,t)\right], \end{aligned} \tag{9}$$

where the tilde-accented transport coefficients are with respect to transient resonances and $\mathcal{Q}$ is the transition rate for phase trapping process only. Using Hamiltonian perturbation theory, Artemyev et al. (2016, 2017), Artemyev, Neishtadt, Vainchtein, et al. (2018), and Artemyev, Neishtadt, Vasiliev, et al. (2018) obtained analytical expressions for the transport coefficients and the function $\mathcal{Q}$ in equation (9) for constant monochromatic plasma waves of various kinds. Under their particular wave assumptions, $\mathcal{Q}$ reduces to a Dirac-delta function so that equation (9) degenerates to a differential equation and is easily solved. Though they had apparently put $\tilde{B}_I$ in place of $\tilde{h}_I$ in their equations, their solutions nonetheless agreed well with test particle results, possibly due to domination of the phase trapping terms.

3. Simulation Methods

In this paper, we will simulate energetic electron distribution evolutions in both monochromatic and broadband EMIC wavefields in a realistic cold plasma background in Earth's dipole field. Since EMIC waves could be strong, our simulation mainly relies on the Green's function method based on numerically integrating a Chapman-Kolmogorov equation like that in equation (1), although the coordinate is conveniently a particle's equatorial pitch angle α_0. Discretization of the Green's functions results into a stochastic matrix named the Markov matrix and hence a Markov chain (e.g., Doob, 1953) description of the wave-particle interaction processes. The Green's functions are evaluated from test particle simulations within the wavefield for a time interval comparable to electron bounce period. We will give a detailed account of the wave setup and test particle simulation in section 3.1. It is known that wave incoherence could interrupt phase trapping process and hence produce less particle transport than expected from coherent wave (Artemyev et al., 2012;

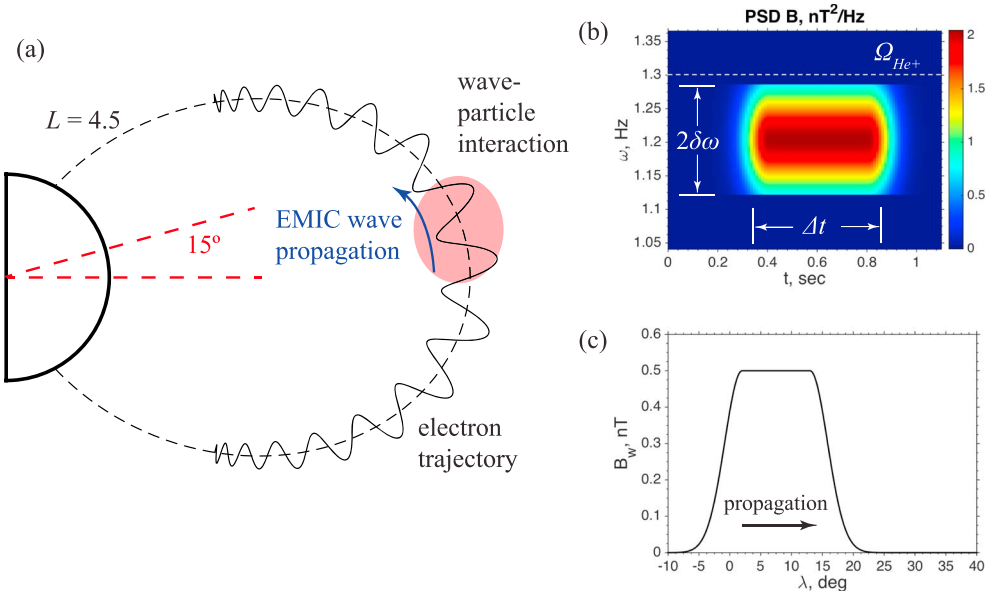

Figure 1. (a) Schematic illustration of the test particle simulation setup. Electromagnetic ion cyclotron (EMIC) wave packet is confined below 15° latitude in the Northern Hemisphere, and wave-particle interaction occurs within this region (pink). (b) Example power spectral density of a broadband wave packet, with parameters $B_w^{\mathrm{rms}} = 0.5$ nT, $\omega_m = 3.7\,\Omega_{O+}$, and $\delta\omega = 0.25\,\Omega_{O+}$ (see text for meaning of the parameters). Wave power is gradually turned on and off and lasts for a nominal time period $\Delta t = 0.5$ s. White dashed line indicates He^+ gyrofrequency. (c) Latitudinal variation of wave magnetic amplitude. PSD B = magnetic power spectral density

Tao et al., 2012). Therefore, we will also compare the Green's function method results with solutions from the presumed Fokker-Planck equation (6), to see under what conditions the interrupted nonlinear transport effect could be so small that it guarantees Kramer-Moyal expansion for the integral term in equation (9) as well and hence allows for a Fokker-Planck approximation of the master equation as a whole. The numerical methods are described in section 3.2.

3.1. Test Particle Simulation

We study energetic electron interaction with L-mode He^+ band EMIC waves at geocentric distance $L = 4.5$, which is a typical L value of strong He^+ band emissions where the minimum electron resonant energy could be less than 2 MeV (Meredith et al., 2003). The test particles interact with EMIC waves in a certain latitudinal range (0–15°, see Figures 1a and 1c), whose dynamics could be solved in principle by the Newton-Lorentz equations:

$$\frac{\mathrm{d}\boldsymbol{p}}{\mathrm{d}t} = -e\left[\boldsymbol{E}_w + \frac{1}{\gamma m_e}\boldsymbol{p}\times(\boldsymbol{B}_w + \boldsymbol{B}_0)\right], \tag{10}$$

$$\frac{\mathrm{d}\boldsymbol{r}}{\mathrm{d}t} = \frac{1}{\gamma m_e}\boldsymbol{p}, \tag{11}$$

where e is the absolute value of elementary charge, m_e is electron rest mass, γ is the Lorentz factor, r and p are electron's position and momentum, E_w and B_w are electric and magnetic components of the wavefield, and B_0 is the background geomagnetic field. In actual simulation, gyro-averaged formalism of equations (10) and (11) is employed, and the gyro-averaged equations can be found from, for example, Chang and Inan (1983) and Li et al. (2015).

The EMIC wave is assumed to propagate parallel along Earth's dipole field line, from magnetic equator toward Northern Hemisphere. Ambient cold plasmas are consisted with electrons, protons, and heavy ions, with a typical storm time ion composition of 70% H^+, 20% He^+, and 10% O^+. The ratio between equatorial electron plasma frequency and gyrofrequency (ω_{pe}/Ω_e) is 15, which gives an equatorial electron number density $n_{e0} = 255$ cm^{-3} typical for the outer plasmasphere (Meredith et al., 2003). Variation of electron number density with magnetic latitude then takes the empirical form $n_e = n_{e0}\cos^{-4}\lambda$ (Bortnik et al., 2008).

With these parameters and a prescribed wave magnetic component, the wave electric component and wave number are computed according to the cold plasma dispersion relation (e.g., Stix, 1962).

Figure 1b plots magnetic power spectral density for an example broadband wave packet. The wave packet has a root-mean-square magnetic amplitude $B_w^{\rm rms} = 0.5$ nT and a Gaussian-shaped spectrum $P_w(\omega) \propto \exp[-(\omega-\omega_m)^2/\delta\omega^2]$, with median frequency $\omega_m = 3.7\,\Omega_{O+}$, nominal half bandwidth $\delta\omega = 0.25\,\Omega_{O+}$, and two cutoff frequencies at 3.45 and 3.95 Ω_{O+}, respectively. The wave packet is numerically represented by 101 discrete monochromatic wave elements with frequencies linearly spanning between the two cutoffs and randomized initial phases. Throughout this work, ω_m is a fixed parameter, and all broadband wave packets have the same $\delta\omega = 0.25\,\Omega_{O+}$.

For the purpose of calculating a Green's function $P(\alpha_0, \Delta t|\alpha_0')$, wave power is temporally confined to a nominal time period $\Delta t = 0.5$ s, which is comparable to test particle bounce period to ensure that every particle interacts with wave once. Smoothing tapers are imposed on both edges of temporal (Figure 1b) as well as spatial (Figure 1c) confinement of the wave packet in order to minimize nonresonant wave-particle interaction effects induced by abrupt variations of the wavefield (Chen et al., 2016). An ensemble of electrons, with common initial α_0' and evenly distributed gyrophase and bounce phase (36×48), are released at $t = 0$ s and traced till the complete shutdown of waves. These electrons bounce between magnetic mirror points or surface of Earth if in the bounce loss cone. Electron atmospheric loss is not contained in the Green's functions in order to abide by the property (A2) but is treated in the simulation algorithms (next subsection). From their final distribution in α_0, the probability density $P(\alpha_0, \Delta t|\alpha_0')$ is then obtained. In our test particle simulations, the Green's functions are evaluated every 0.25° for α_0' from 0.25° to 90°.

3.2. Numerical Algorithms

Ignoring atmospheric loss temporarily, with the Green's functions $P(\alpha_0, \Delta t|\alpha_0')$ obtained for every α_0', the distribution function $F(\alpha_0, t)$ can be repeatedly evolved by a Chapman-Kolmogorov equation like equation (1) in the α_0 coordinate. For EMIC waves, α_0 is a more convenient coordinate than the first two adiabatic invariants because the problem can thereby be regarded as one dimensional. In this coordinate, $F(\alpha_0, t)$ is different from phase space density (PSD), which we shall denote by $f(\alpha_0, t)$, since $F(\alpha_0, t)\mathrm{d}\alpha_0$ gives the number of particles in $\mathrm{d}\alpha_0$ but $\mathrm{d}\alpha_0$ is not a phase space element. Instead, they are related by a Jacobian factor as

$$F(\alpha_0, t) = f(\alpha_0, t)G(\alpha_0), \tag{12}$$

with $G(\alpha_0) \approx (1.38 - 0.64\sin^{3/4}\alpha_0)\sin(2\alpha_0)$ (Davidson, 1976). Discretization of the Chapman-Kolmogorov equation results into a matrix equation

$$\mathbf{F}^{(n+1)} = \mathbf{F}^{(n)}\mathbf{P}, \tag{13}$$

in which the state vector of the nth time step $\mathbf{F}^{(n)}$ is a row vector (called stochastic vector), with each of its element giving the number of particles in an α_0 element, and the square matrix $\mathbf{P}$ is called a Markov matrix. Row dimension of $\mathbf{P}$ represents the initial coordinate α_0', and column dimension represents the final coordinate α_0. The i-j element of $\mathbf{P}$ (P_{ij}) gives the probability of a stochastic process traveling from an α_0' position indexed by i to an α_0 position indexed by j in Δt time. Each row of $\mathbf{P}$, therefore, is a discretization of the Green's function $P(\alpha_0, \Delta t|\alpha_0')$ for a specific α_0', and the two properties of the Green's function (A1) and (A2) now become $P_{ij} \geqslant 0$ and $\sum_j P_{ij} = 1$ for all i and j.

If we interpret $\mathbf{P}$ as a transport operator onto $\mathbf{F}^{(n)}$ in equation (13), we may also treat the atmospheric loss as another operator $\mathbf{L}$, and let these two operations take place in sequence:

$$\mathbf{F}^{(n+1)} = \mathbf{F}^{(n)}\mathbf{L}\mathbf{P}. \tag{14}$$

In general, the two operators do not commute, but we choose such an order because for finite Δt and sharply defined loss cone, the operator $\mathbf{L}$ would introduce a discontinuity into the distribution at the loss cone edge, and a subsequent operation by $\mathbf{P}$ could smear it out. For large powers of the product $\mathbf{LP}$, however, their particular order makes virtually no difference to the evolution process.

The matrix $\mathbf{L}$ must be diagonal since atmospheric loss is an in situ process in α_0 coordinate. For α_0 out of the bounce loss cone, no loss occurs and $L_{ii} = 1$; for α_0 inside the bounce loss cone, a simple treatment is to take $L_{ii} = \exp(-\Delta t/\tau)$ since it resembles the solution of the loss equation

$$\frac{\mathrm{d}F}{\mathrm{d}t} = -\frac{F}{\tau}, \tag{15}$$

with a life time τ equal to one half of a bounce period T_b. Throughout this work, the loss cone angle $\alpha_{0L} \approx 4.4°$, which is derived from the dipole $L = 4.5$, and T_b takes a uniform value 0.5 s for simplicity of calculation. More sophisticatedly, we may let $\mathbf{L}$ operate on both $\mathbf{F}^{(n)}$ and $\mathbf{F}^{(n+1)}$, and hence, write the loss process alone in an implicit manner:

$$\mathbf{F}^{(n+1)} = \kappa \mathbf{F}^{(n+1)}\mathbf{L} + (1-\kappa)\mathbf{F}^{(n)}\mathbf{L}, \tag{16}$$

where κ is an adjustable parameter between $[0, 1)$ that takes the value $1/2$ in this work. Equation (16) yields an implicit loss operator $\widetilde{\mathbf{L}} = (1-\kappa)\mathbf{L}(\mathbf{I} - \kappa\mathbf{L})^{-1}$, where $\mathbf{I}$ is identity matrix, which leads to the following matrix evolution equation

$$\mathbf{F}^{(n+1)} = \mathbf{F}^{(n)}\widetilde{\mathbf{L}}\mathbf{P} = \mathbf{F}^{(0)}(\widetilde{\mathbf{L}}\mathbf{P})^{n+1}, \tag{17}$$

in which $\mathbf{F}^{(0)}$ is provided by initial condition.

For a typical simulation of evolution, the matrix power in equation (17) would be of the order 10^2–10^3. Large powers of a large matrix often invoke oscillatory or divergent behavior in the resultant state vector due to even tiny numerical errors in the matrix eigenspectrum. A major source of these errors, however, lies in the discretization itself, that is, trying to represent an infinite-dimensional state space by but a finite number of dimensions (360 in this work). To stabilize the algorithm, we thus introduce an additional operator $\mathbf{H}$ after $\widetilde{\mathbf{L}}\mathbf{P}$, which mixes adjacent elements of the state vector in the manner $F_i^{(n)} = (F_{i-1}^{(n)} + F_{i+1}^{(n)})/2$ for all indices i where the operation $\widetilde{\mathbf{L}}\mathbf{P}$ is nonsingular; that is, the Green's function is not a Dirac-delta function. For α_0's where the Green's function is a Dirac-delta function, no mixture is needed whatsoever because temporal evolution of the distribution function there does not depend on its neighbors. Therefore, the matrix representation of $\mathbf{H}$ might be something like this:

$$\mathbf{H} = \begin{pmatrix} 1 & & & & & \\ & 1 & & & & \\ & & 1/2 & 1/2 & & \\ & & 1/2 & 0 & 1/2 & \\ & & & 1/2 & 0 & \ddots \\ & & & & \ddots & \ddots \end{pmatrix}, \tag{18}$$

in which example the first two columns correspond to singular Green's functions and "mixture" begins from the third column. It is evident that such an operation conserves the total number of particles and in effect introduces an artificial diffusion with equivalent diffusion rate $(\Delta\alpha_0)^2/(2\Delta t)$ that vanishes as the discretization spacing $\Delta\alpha_0$ approaches 0. Admittedly, $\mathbf{H}$ still depends on a specific discretization and thus cannot fully eliminate numerical errors thereby associated, but our numerical experiments nonetheless speak for its effectiveness. After all these considerations, the final matrix evolution equation in our algorithm is

$$\mathbf{F}^{(n+1)} = \mathbf{F}^{(n)}\widetilde{\mathbf{L}}\mathbf{P}\mathbf{H}. \tag{19}$$

If the kinetic transport can be approximated by a Fokker-Planck equation, changing coordinate from I to α_0 in equation (6) and taking into account the bounce loss term, we have

$$\frac{\partial}{\partial t} f = -\frac{1}{G}\frac{\partial}{\partial \alpha_0}\left(G h_\alpha f\right) + \frac{1}{G}\frac{\partial}{\partial \alpha_0}\left(G D_{\alpha\alpha}\frac{\partial}{\partial \alpha_0} f\right) - \frac{1}{\tau} f, \tag{20}$$

with

$$\tau(\alpha_0) = \begin{cases} \frac{1}{2}T_b, & (\alpha_0 \leqslant \alpha_{0L}), \\ +\infty, & (\alpha_0 > \alpha_{0L}), \end{cases} \tag{21}$$

exactly the same as that in $\widetilde{\mathbf{L}}$. Under quasi-linear approximation, whereby the term with h_α in equation (20) vanishes identically, we are allowed to validate the above described Green's function method against solutions of equation (20) with input quasi-linear diffusion coefficients (e.g., Glauert & Horne, 2005). Using the same plasma and wave parameters as exemplified in section 3.1, the quasi-linear diffusion equation solutions are obtained for 2-MeV electrons with the initial condition:

$$f(\alpha_0, 0) = \begin{cases} 0, & (\alpha_0 \leqslant \alpha_{0L}), \\ \sin(\alpha_0) - \sin(\alpha_{0L}), & (\alpha_0 > \alpha_{0L}), \end{cases} \tag{22}$$

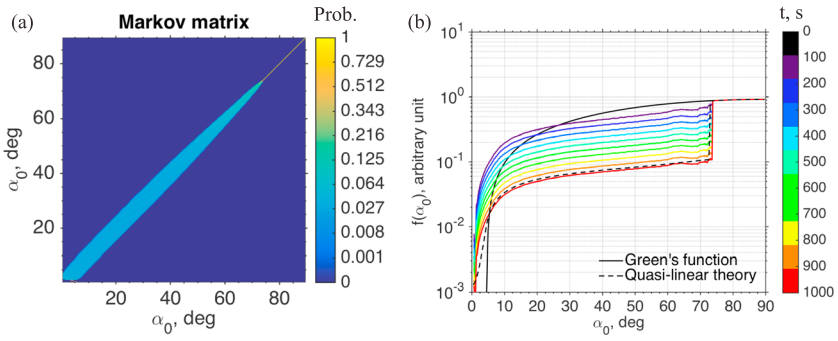

Figure 2. (a) Pseudo color plot of Markov matrix inferred from electromagnetic ion cyclotron wave quasi-linear diffusion coefficients, with wave parameters $B_w^{\rm rms} = 0.5$ nT, $\omega_m = 3.7\,\Omega_{O+}$, and $\delta\omega = 0.25\,\Omega_{O+}$, for 2-MeV electrons. (b) Phase space density solutions obtained from both Green's function method (solid) at a series of time stamps (color coded) and quasi-linear theory (dashed) at $t = 1,000$ s.

and reflective boundary conditions on both ends of α_0. For the Green's function method, the corresponding Green's functions $P(\alpha_0, \Delta t|\alpha_0')$ are inverted from the known diffusion coefficients and the null advection coefficients using equations (4), (5), and (7), transformed into α_0 coordinate, for a finite $\Delta t = 0.5$ s. To evaluate the integrals in equations (4) and (5), we assume a square function shape of $P(\alpha_0, \Delta t|\alpha_0')$ for simplicity. Median and width of the square function can then be analytically solved from these equations, and the Green's function is finally determined after normalization. Following the discretization procedure, the Markov matrix **P** is obtained as plotted in Figure 2a, and solutions from both methods are compared as in Figure 2b. Overall, the Green's function solution at $t = 1,000$ s agrees remarkably well with that of the quasi-linear Fokker-Planck equation, and the algorithm appears to be quite stable after the 2,000th power of a matrix. We notice some artifacts in the Green's function solutions at $\alpha_0 \sim 0$ in Figure 2b. These are caused by the fact that width of the square function has no real root from equations (4), (5), and (7) at very small α_0 due to the finite Δt, and as a remedy the Green's functions there are simply replaced by Dirac-delta functions at their respective median positions (see Figure 2a near the bottom edge). However, this artifact will not exist for Green's functions calculated from test particles.

4. Simulation Results

4.1. Markov Matrix and Transport Coefficients

Although Fokker-Planck equation may not always be a valid approximation to the master equation for nonlinear wave-particle interactions, we could still find useful information from the calculated transport coefficients when they are compared with quasi-linear predictions. Figure 3 shows three examples of the Markov matrix and transport coefficients calculated for 5-MeV test electrons in a monochromatic EMIC wavefield with $B_w^{\rm rms} = 0.5$ nT (a–c), in a counterpart broadband wavefield (d–f), and in broadband wavefield with ensemble-averaged wave initial phases (g–i). In the last case, the Markov matrix is an arithmetic mean over six Markov matrices individually obtained with the same broadband wave parameters but differently randomized wave initial phases, including the one shown in Figure 3d. Wave phase average is unnecessary for the monochromatic wavefield, because in that case there is only one wave element, and its initial phase makes no difference to test particle results due to the even distribution of particle gyrophases. Test particle transport coefficients, including the drift coefficients (B_α), diffusion coefficients ($D_{\alpha\alpha}$), and advection coefficients (h_α), are calculated according to equations (4), (5), and (7) in the α_0 coordinate using a finite $\Delta t = 0.5$ s. In comparison, quasi-linear diffusion coefficients are provided by the method in Glauert and Horne (2005), and quasi-linear drift coefficients are inferred from equation (7) by vanishment of advection coefficients in quasi-linear theory.

In the monochromatic wave case, test particle diffusion coefficients (Figure 3b) closely follow the quasi-linear ones except in a narrow range of α_0 between 60° and 70°, which is the range of nonlinear wave-particle interaction. The nonlinear behaviors are more clearly seen as the oscillations of h_α in Figure 3c. The positive and negative peaks in h_α are results of the competition between phase bunching and phase trapping effects, because EMIC wave phase bunching only transports electrons toward greater α_0's and phase trapping only toward loss cone (Albert & Bortnik, 2009). Outside of the nonlinear α_0 range, h_α nearly remains 0, indicating that wave-particle interaction there is well approximated by quasi-linear diffusion. These non-

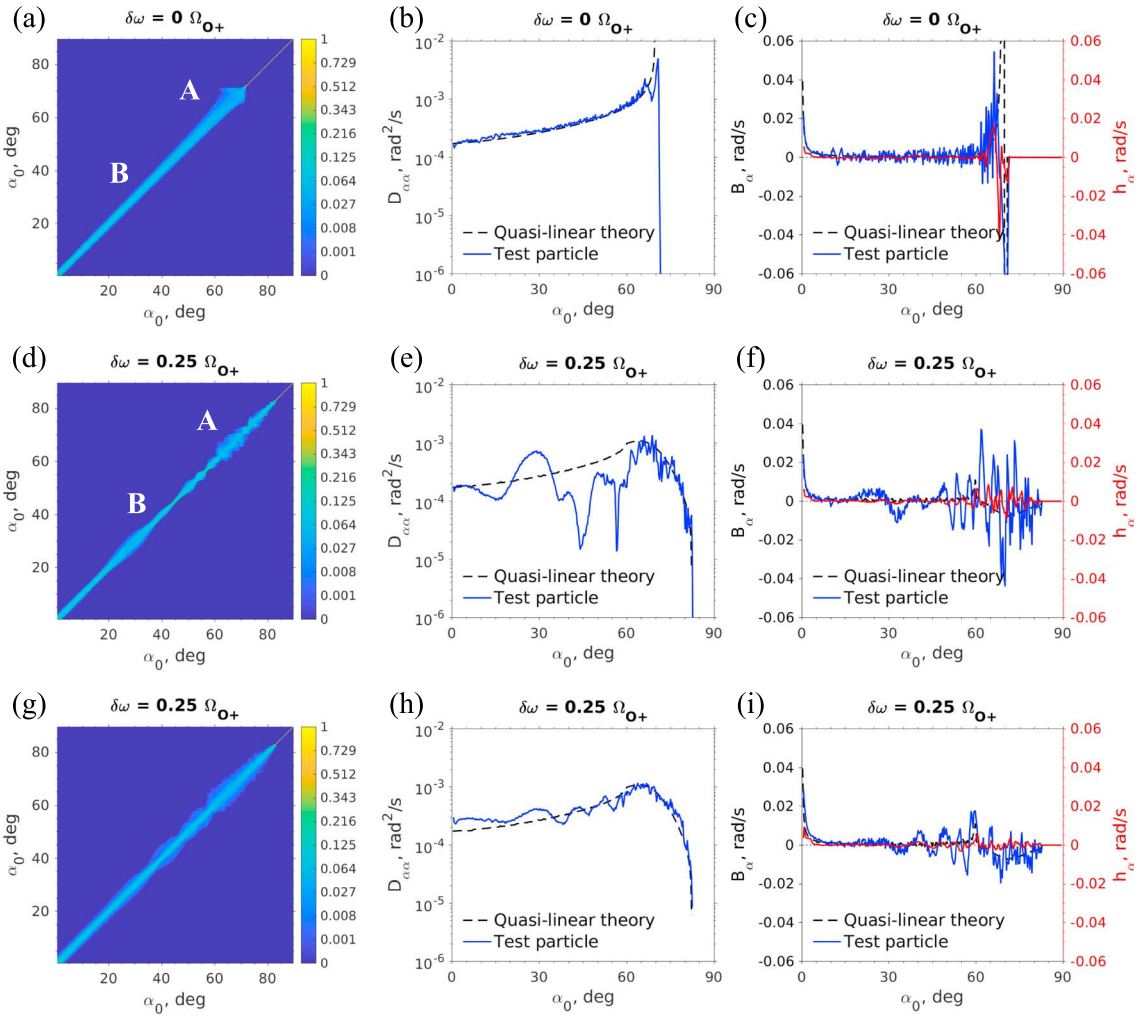

Figure 3. (a) Markov matrix for 5-MeV electrons in a monochromatic electromagnetic ion cyclotron wavefield with $B_w^{\mathrm{rms}} = 0.5$ nT. Letter "A" indicates the portion of Green's functions that shows nonlinear wave-particle interaction effects; letter "B" indicates the portion that characterizes quasi-linear diffusion. (b) Diffusion coefficients ($D_{\alpha\alpha}$) from quasi-linear theory (dashed black) and test particle simulation (solid blue). (c) Left y axis: drift coefficients (B_α) inferred from quasi-linear theory (dashed black) and calculated by test particle simulations (solid blue); right y axis: advection coefficients (h_α) for test particle simulation (solid red). (d–f) Same as (a)–(c) but for a broadband EMIC wavefield. (g–i) Ensemble-averaged results over six broadband test particle simulations with the same parameters as in (d)–(f) but different wave initial phases.

linear and quasi-linear behaviors are also characterized in the Markov matrix (Figure 3a), where they are marked by the letters "A" and "B," respectively. Near letter A, the Green's functions are apparently biased either toward smaller α_0 due to phase trapping effect, or toward larger α_0 due to phase bunching effect; whereas near letter B, the Green's functions behave much like those inferred from quasi-linear diffusion coefficients (cf. Figure 2a).

In the broadband wave case, test particle diffusion coefficients (Figure 3e) deviate around the quasi-linear ones in the α_0 range about 10° to 60°. However, this disparity is not a result of nonlinear wave-particle interaction, as can be revealed from the vanishing h_α in this range in Figure 3f. The pattern of these deviations is related to the specific initial phases of the wave elements in the broadband wave packet. In the Markov matrix (Figure 3d), the Green's functions near letter A do not show clear bias as in the monochromatic case, suggesting that phase trapping and phase bunching are interrupted by the finite wave bandwidth. The interruption of nonlinear wave-particle interaction effects is also indicated by the weaker h_α oscillations in the nonlinear α_0 range in Figure 3f compared to those in Figure 3c.

In the wave phase-averaged broadband case, the Markov matrix (Figure 3g) exhibits more resemblance to that inferred from quasi-linear theory, and the test particle calculated diffusion coefficients (Figure 3h) agree

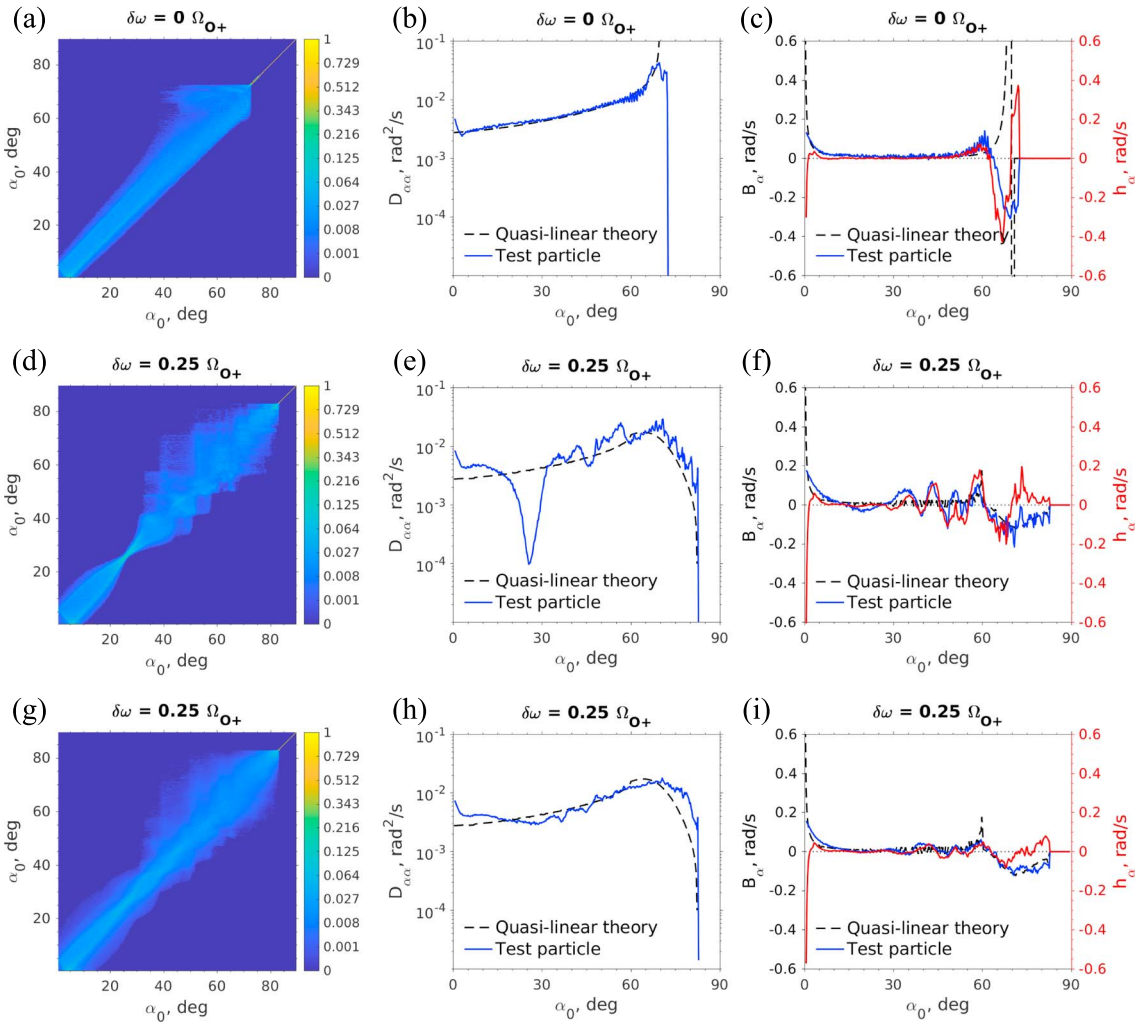

Figure 4. Same as Figure 3 but for $B_w^{\mathrm{rms}} = 2$ nT wavefields.

reasonably well with the quasi-linear predictions. This agreement on the one hand confirms that quasi-linear theory is a good approximation for small-amplitude and incoherent waves and on the other hand demonstrates that the disparity of $D_{\alpha\alpha}$ in Figure 3e is indeed a result of the specific wave initial phases. In Figure 3i, test particle calculated B_α weakly oscillates around the quasi-linear predictions, and h_α shows very little wiggling, compared to that in Figure 3f, as an indication of approaching to quasi-linear theory. It is noteworthy that the positive bump in h_α at $\alpha_0 \sim 0$ is unaffected by the wave phase average. This bump is caused by the particle boundary reflection effect (Inan et al., 1978; Su et al., 2012) not contained in quasi-linear theory, which also leads to the slightly greater $D_{\alpha\alpha}$ at $\alpha_0 \sim 0$ evaluated by test particles in Figure 3h.

Figure 4 shows the Markov matrices and transport coefficients for 5-MeV electrons in $B_w^{\mathrm{rms}} = 2$ nT EMIC wavefields, in the same format as Figure 3. With stronger wave amplitudes, electrons undergo stronger scatterings as seen from the Markov matrices in Figures 4a, 4d, and 4g compared to those in Figure 3. In Figures 4c and 4f, the α_0 ranges of nonvanishing h_α are wider than those in the weak wave counterparts, indicating wider ranges of nonlinear wave-particle interaction when the wave becomes stronger. This α_0 range in the monochromatic case (Figure 4c) is qualitatively consistent with those estimated by the nonlinear inhomogeneity parameter as in, for example, Albert and Bortnik (2009) and Su et al. (2012). The singularity in h_α at $\alpha_0 = 0$ in Figures 4c, 4f, and 4i is a result of the vanishing Jacobian factor to transform equation (7) from canonical coordinate to α_0 there, which was not resolved in the weak wave cases by the finite $\Delta\alpha_0'$ (=0.25°) in launching test particles. In Figures 4g–4i, strong nonlinear interaction effects survived the wave phase average and exhibit in h_α the oscillations between $\alpha_0 \sim 65°$ and 80°. The stronger electron

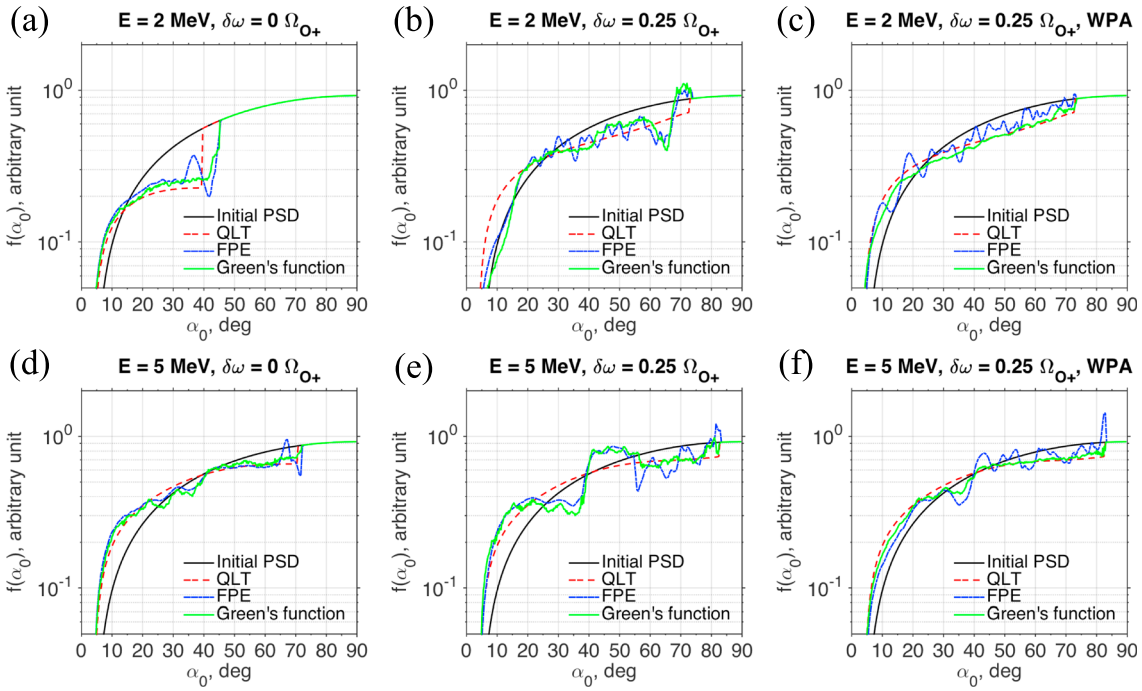

Figure 5. Phase space density (PSD) results at $t = 200$ s obtained from quasi-linear theory (QLT, dashed red), advective Fokker-Planck equation (FPE, dash-dotted blue), and Green's function method (solid green), for (a–c) 2-MeV and (d–f) 5-MeV electrons in $B_w^{\rm rms} = 0.5$ nT electromagnetic ion cyclotron wavefields. Initial PSD is indicated by solid black line. The wavefield is monochromatic in (a) and (d), broadband in (b) and (e), and broadband and wave phase averaged in (c) and (f).

transport due to nonlinear effects also cause the larger test particle $D_{\alpha\alpha}$ than quasi-linear predictions in this α_0 range (Figure 4h).

4.2. PSD and Precipitation Flux

Figure 5 shows the PSDs evolved after 200 s from a common initial condition as in equation (22) for 2- and 5-MeV electrons in weak EMIC wavefields with $B_w^{\rm rms} = 0.5$ nT. The wavefield is monochromatic in Figures 5a and 5d, broadband in Figures 5b and 5e, and wave phase-averaged in Figures 5c and 5f. In each panel, the PSDs are obtained from three different ways: (i) the Green's function method described in section 3, (ii) solution of the presumed advective Fokker-Planck equation (20) obtained using a flux conservative finite difference solver (e.g., Ames, 2014) with transport coefficients evaluated by test particles, and as a reference (iii) solution of the quasi-linear diffusion equation with quasi-linear diffusion coefficients. For the 5-MeV cases (Figures 5d–5f), the Markov matrices and corresponding transport coefficients used are those shown in Figure 3.

For monochromatic wave (Figures 5a and 5d), the advective Fokker-Planck solutions could closely reproduce those from the Green's function method at most α_0's, except in a small range where the Fokker-Planck equation falsely predicts PSD peak and trough that are not seen in the latter. From the last subsection, we know that this is the α_0 range in which nonlinear wave-particle interaction takes place, and Fokker-Planck approximation fails herein due to the corresponding large stochastic changes. Particle transport in the Fokker-Planck approximation is a local process in which the particles are only allowed to move a small distance in a small time period and thus may accumulate or rarefy along their transport. However, the transport by nonlinear wave-particle interaction is more like a jumping process, and from the Green's function method results we find that it actually does not generate peak or trough in the distribution. Except for a minor difference in resonance α_0 range in Figure 5a, in general the Green's function method results are pretty close to the quasi-linear theory predictions. This agreement suggests that, although nonlinear transport is faster than quasi-linear diffusion, the opposite effects of phase bunching and phase trapping generally cancel each other, and the resultant PSD evolution is not significantly different from quasi-linear diffusion.

In the broadband wave cases (Figures 5b and 5e), PSD pitch angle structures are developed in solutions from both the advective Fokker-Planck equation and the Green's function method, and the two results

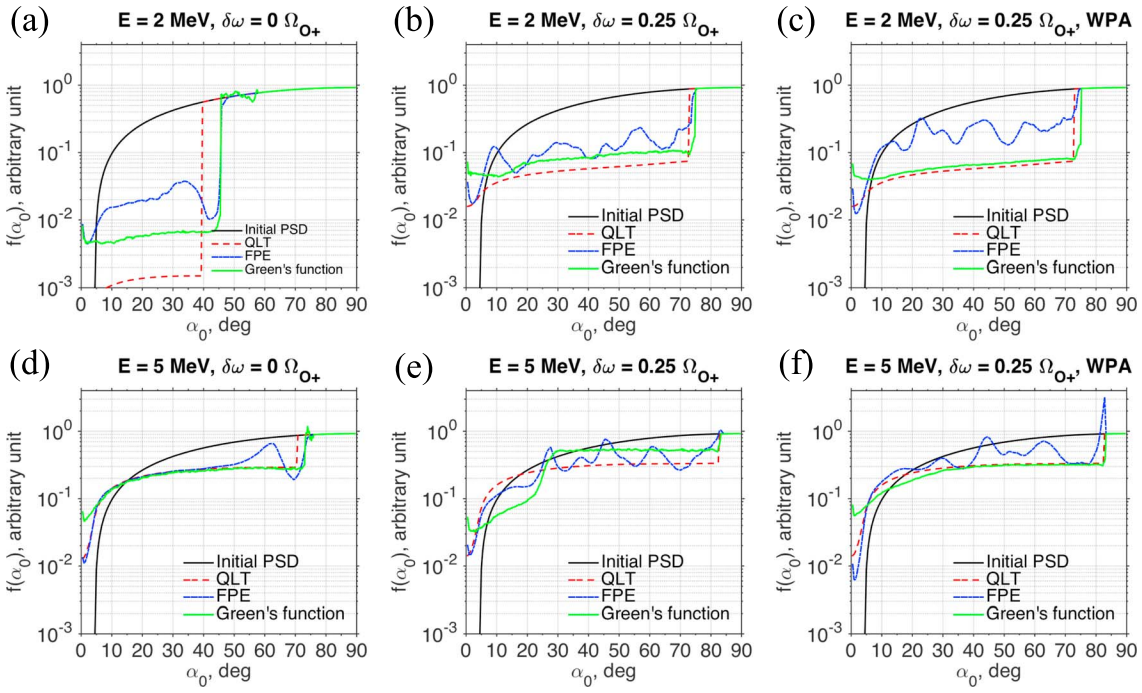

Figure 6. Same as Figure 5 but for $B_w^{\mathrm{rms}} = 2$ nT wavefields.

largely agree with each other except for minor details. This agreement suggests that, when the wave amplitude is small and spectrum is broadband, the master equation could be adequately approximated by a Fokker-Planck equation in the entire α_0 range. Quasi-linear theory, which contains only diffusive transport, is unable to show any pitch angle structure in its solutions. We remark that these PSD pitch angle structures depend on the relative phase differences between wave elements; thus, for a different set of random wave initial phases, locations of the maxima and minima will also be different. This phenomenon is a consequence of calculating the Markov matrix from just one cycle of test particles interacting with one wave packet. Physically, repetitive convolution of such a Markov matrix implies that the electrons would always encounter the wave packet in their subsequent bounces with the same phase differences between wave elements, which effectively adds a degree of coherence to the wave packet and might be unrealistic for EMIC waves. On the other hand, this also gives us a hint on what to expect for electrons interacting with weak and coherent waves. For monochromatic wavefield, this phenomenon is absent because there is only one wave element.

In the wave phase-averaged cases (Figures 5c and 5f), the aforementioned effective wave coherence is largely removed; thus, the PSD pitch angle structures disappear, and both the Green's function and the advective Fokker-Planck equation solutions show consistency with quasi-linear theory. The sharp peak in the 5-MeV electron advective Fokker-Planck equation solution (Figure 5f) at the intersection between resonance and nonresonance ($\alpha_0 \approx 82°$) is numerically caused by the discontinuities in $D_{\alpha\alpha}$ and h_α there.

Figure 6 shows PSD solutions in the same format as Figure 5 but for $B_w^{\mathrm{rms}} = 2$ nT wavefields, which are intense enough to reach the strong diffusion limit in quasi-linear theory and hence result in a filled bounce loss cone. The 5-MeV electron results (Figures 6d–6f) are obtained using the Markov matrices and transport coefficients shown in Figure 4. In contrast to the weak wave situation, advective Fokker-Planck equation in this case unexceptionally gives very different solutions from the Green's function method; therefore, Fokker-Planck approximation to the master equation is totally invalid for large-amplitude waves. Comparing Figures 6b and 6e with Figures 5b and 5e, in the strong broadband wave cases, the lack of PSD pitch angle structures in the Green's function method results suggests that electron transport is now too fast to be described by advection and diffusion processes, which caused the pitch angle structures in the weak wave counterparts. The effective wave coherence again makes the Green's function method yield different solutions from quasi-linear theory.

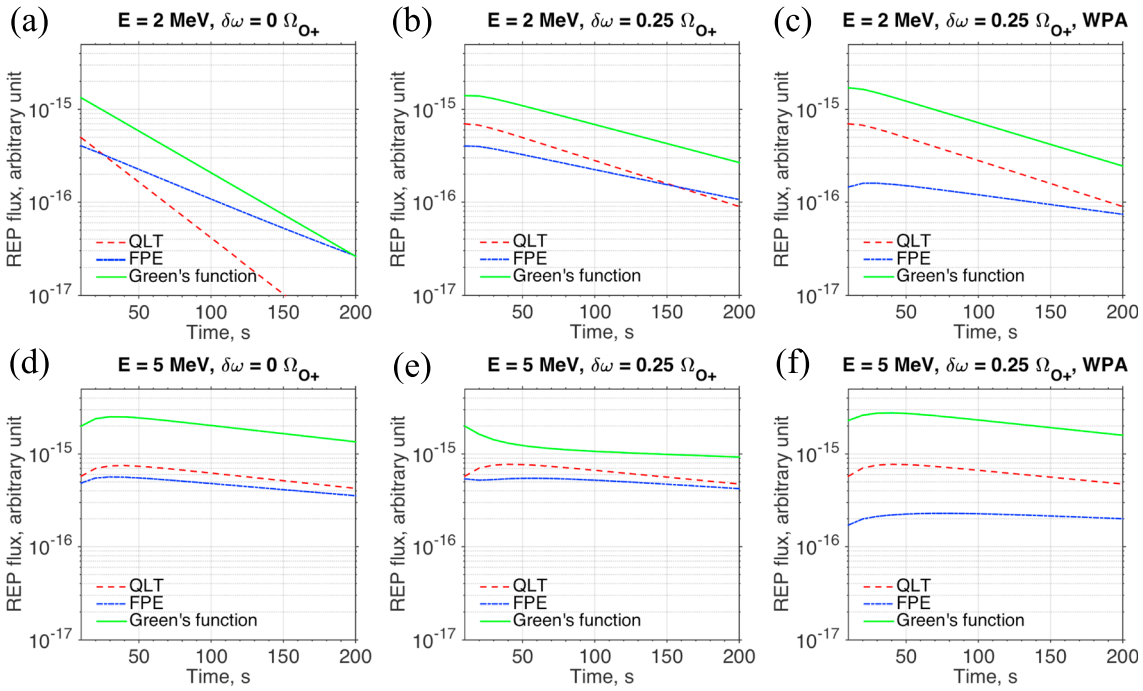

Figure 7. Temporal evolution of relativistic electron precipitation (REP) fluxes calculated from the corresponding phase space density solutions in Figure 6 , for (a-c) 2-MeV and (d-f) 5-MeV electrons in (a and d) monochromatic wavefield, (b and e) broadband wavefield, and (c and f) broadband and wave phase-averaged wavefield. Note that time in these panels starts from 10 s rather than 0 s, because at $t = 0$ s the REP flux is zero due to the initially empty loss cone. QLT = quasi-linear theory; FPE = Fokker-Planck equation.

In the wave phase-averaged scenario (Figures 6c and 6f), it is interesting to notice that, although the Fokker-Planck approximation is no longer valid, quasi-linear theory still gives agreeable results with the Green's function method in a vast range of α_0 far from the loss cone. We note that a pure diffusion equation (with only a diffusion term on the right) is in fact free from the small stochastic change restriction, because a reduction of time scale in such an equation can always bring the corresponding stochastic changes small enough without altering the form of its solution. But with the added loss term, which has a specific time scale, it no longer has this freedom, and this is why quasi-linear theory starts to deviate from the Green's function method solutions near the loss cone. The physical manifestation is that electrons are piled up in the loss cone in all the Green's function method solutions, leading to fuller loss cones than quasi-linear theory predictions and peculiar negative PSD slopes. The same thing also happens for the monochromatic case in Figure 6d. From Figures 4c and 4i we know that it is out of the α_0 range of nonlinear wave-particle interaction near the loss cone, and nonlinear transport has been largely reduced by wave phase average. Therefore, these peculiar loss cone PSD structures are simply caused by the large stochastic changes due to intense wave rather than by nonlinear interaction.

The peculiar loss cone PSD shapes in the Green's function results all lead to stronger relativistic electron precipitation (REP) fluxes, which are observable by sounding balloons (e.g., Woodger et al., 2015), than quasi-linear theory. Figure 7 plots temporal evolutions of the REP fluxes corresponding to the PSD solutions in Figure 6. The REP fluxes are calculated according to the formula (e.g., Li et al., 2013; Lyons & Williams, 1984)

$$j_{\mathrm{REP}}(E,t) = 2\pi\sqrt{4L^6 - 3L^5}\int_0^{\frac{1}{2}\alpha_{0L}} j_0(\alpha_0, E, t)\frac{(1-\sin^2\alpha_0)^{\frac{1}{2}}\sin\alpha_0}{[1-(4L^6-3L^5)^{\frac{1}{2}}\sin^2\alpha_0]^{\frac{1}{2}}}\mathrm{d}\alpha_0, \tag{23}$$

where j_0 is the equatorial electron flux obtained from the PSD solution, and the integration is performed from $\alpha_0 = 0$ to $\alpha_{0L}/2$ rather than α_{0L} to roughly take into account that only electrons with small enough α_0 within bounce loss cone could reach the altitude of sounding balloons (Marshall & Bortnik, 2018). In all the panels, the REP fluxes inferred from the Green's function method are generally several times stronger than the predictions from quasi-linear theory. The advective Fokker-Planck equation method does not qual-

Table 1
Normalized Total Electron Content at $t = 200$ s

Panel[a]	QLT	FPE	Green's function
a	0.724	0.623	0.615
b	0.210	0.309	0.234
c	0.210	0.453	0.198
d	0.561	0.604	0.522
e	0.535	0.661	0.758
f	0.535	0.769	0.495

Note. FPE = Fokker-Planck equation; QLT = quasi-linear theory.
[a]Referring to panels in Figure 6.

itatively improve its predictions on REP fluxes over quasi-linear theory, because for large amplitude waves Fokker-Planck approximation breaks down.

Electron loss rates can be assessed by the total electron content (TEC) evaluated by integrating $f(\alpha_0)G(\alpha_0)\mathrm{d}\alpha_0$. Table 1 gives the TECs calculated using the PSD solutions in Figure 6 normalized to their common initial value. In the wave phase-averaged situations (Figures 6c and 6f, as well as in Figure 6d), the Green's function method gives slightly faster decreases in TECs than quasi-linear theory due to the fuller loss cone, but the differences are rather insignificant compared to the amounts of decrease. This can also be perceived from the proximity of the Green's function method and quasi-linear theory solutions shown in these panels. Therefore, it seems that nonlinear wave-particle interaction does not significantly change the electron loss rates estimated by quasi-linear theory. In Figures 6b and 6e, the Green's function method gives slower losses than quasi-linear theory and that shall be attributed to the effective wave coherence. In Figure 6a, quasi-linear theory predicts drastically deeper PSD depletion than the Green's function method. It may appear that quasi-linear theory gives overestimated electron loss than the Green's function method, but the TECs reveal the other way. The paradox is explained by the fact that the test particles have a noticeably wider resonance α_0 range than that in quasi-linear theory, probably due to the fact that, for monochromatic wavefield, quasi-linear theory has a singularity in diffusion coefficients and hence an abrupt transition from resonance to nonresonance (Su et al., 2012), whereas the transition for test particles is gradual (also cf. Figure 4b). As a result, some of the nonresonant electrons in quasi-linear theory become resonant and get lost in the Green's function method and that leads to greater electron loss in the latter.

5. Conclusions and Discussion

Chapman-Kolmogorov equation is the most fundamental equation governing kinetic evolution of stochastic systems. Based on Chapman-Kolmogorov equation and the Markov chain description of stochastic processes, we have presented a simulation method for energetic electron distribution evolutions under nonlinear wave-particle interaction in EMIC wavefields. In the Markov chain description, all information of stochastic transportation is contained in the Markov matrix, which is the discretized form of the Green's function and can be evaluated by test particle simulations in various wave setups and ambient plasma configurations. Therefore, our method (the Green's function method) is a general method for nonlinear wave-particle interaction simulations since it does not impose additional assumptions either on the particles or on the waves. The computational burden of this method is mainly in evaluating the Markov matrix. Once evaluated, evolving the system by convolution of the Markov matrix would be much faster than solving a partial differential equation. However, this method is not very suitable for performing long term (e.g., 1 week) radiation belt simulations due to its relatively small temporal stepsize, which is restricted by the time period of simulating test particles; Fokker-Planck equation does not have this problem.

The Green's function method could be easily generalized to higher-dimensional problems such as electron nonlinear interaction with chorus waves, which involve both α_0 and E dimensions. To construct the Markov matrix for higher-dimensional problems, the stochastic state vector must, however, be kept one dimensional, and this can be implemented by cycling through a coordinate partition of the phase space element-by-element in a specific order, analogous to the linear storage of multidimensional arrays in computer memory. Our algorithm stabilization technique could also be straightforwardly transplanted into

higher dimensions, in which case the "state mixture" occurs among adjacent phase space elements rather than adjacent state vector components.

In presenting our method, we have also displayed the mathematical relation between Chapman-Kolmogorov equation and Fokker-Planck equation, while the latter has long been utilized as a standard tool in quasi-linear wave-particle interaction simulations and is only an approximation to the former under small stochastic change assumption. Advective transport had been proposed by some authors (e.g., Albert & Bortnik, 2009) to describe nonlinear interaction of radiation belt electrons with EMIC waves, and nonlinear advection and diffusion coefficients had been calculated from test particle simulations (e.g., Liu et al., 2012; Su et al., 2012). However, our simulation results indicate that, Fokker-Planck equation, and hence the advective and diffusive transport mechanisms, are only valid descriptions of the nonlinear transport processes when the wave is both weak ($B_w^{\mathrm{rms}} = 0.5$ nT) and broadband ($\delta\omega = 0.25\,\Omega_{O+}$); for either strong or monochromatic EMIC wavefield, Fokker-Planck approximation fails. Yet quasi-linear theory, which only considers diffusion but not advection, can give agreeable PSD evolutions with the Green's function method away from the loss cone, in both weak and intense wavefields when the wave is incoherent or monochromatic, unless when quasi-linear theory predicts a different resonance α_0 range than test particles.

Near the loss cone, quasi-linear theory gives under estimated PSDs in strong EMIC wavefields compared to the Green's function method. Accompanied by loss cone saturation, peculiar negative PSD slopes are also developed inside loss cone in the Green's function method results. Detailed examination (not shown) of our simulation results reveal that these peculiar PSD shapes start to form after the first electron bounce period and sustain as electrons are depleted from the radiation belt. Therefore, formation of these peculiar PSD shapes is a transient process that would be better studied by direct particle simulation rather than statistical evolution. These peculiar loss cone PSD structures may be observable by low-orbit spacecraft with sufficient particle pitch angle resolution. In accordance, the Green's function method calculated atmospheric electron precipitation fluxes are also several times greater than those given by quasi-linear theory. These predictions may be verified from high-altitude sounding balloon observations and data analysis.

There had been uncertainty on the effectiveness of nonlinear EMIC wave-particle interaction in transporting electrons toward loss cone. Though phase trapping scatters electrons toward loss cone more quickly than phase bunching does the other way, electrons are more probably phase-bunched rather than phase-trapped (Albert & Bortnik, 2009). Our results indicate that phase bunching and phase trapping do not significantly change electron loss rate as compared to quasi-linear diffusion. Further, these nonlinear effects do not produce observable PSD pitch angle structure either. Yet, in our broad spectrum and specific wave initial phase simulations, PSD pitch angle structures are developed in weak wavefield, and different electron loss rates than quasi-linear theory are achieved in strong wavefield. These effects are, however, a result of the effective wave coherence introduced by the Markov matrix rather than that of nonlinear wave-particle interaction. They nonetheless suggest that PSD evolution with coherent waves, for example, the consecutive rising-tone chorus emissions reported in Fennell et al. (2014), might be very different from quasi-linear theory predictions, and information on wave phases might be indispensable as well.

Appendix A: From Chapman-Kolmogorov Equation to Fokker-Planck Equation

In this appendix we are concerned with the equations satisfied by the transition probability density $P(y, t_2|x, t_1)$ of a Markov process, which provides the conditional probability $P\mathrm{d}y$ of the process value appearing within $(y, y + \mathrm{d}y)$ at time t_2 given that it was x at time t_1. Further, we assume that the Markov process is time stationary, meaning that its underlying stochastic mechanism does not change with time, so that P is only a function of the time difference $t = t_2 - t_1$, and we therefore denote it $P(y, t|x)$ for short. For simplicity, we consider the process to be one dimensional. Generalization to nonstationary and multidimensional cases is straightforward. Mathematical formalism in this appendix largely follows that in Wang and Uhlenbeck (1945); similar derivations may also be found from other classical or modern monographs (e.g., Chandrasekhar, 1943; Reif, 1965; Zank, 2014).

A few obvious properties of $P(y, t|x)$ are as follows:

$$P(y, t|x) \geqslant 0, \tag{A1}$$

$$\int \mathrm{d}y P(y, t|x) = 1. \tag{A2}$$

By writing $P(y,t|x)$, we have tacitly accepted the definition of a Markov process that the conditional probability of its future state only depends on the observation of its current state but not the full history. This leads immediately to the Chapman-Kolmogorov equation that states

$$P(y,t+\Delta t|x)=\int \mathrm{d}z P(y,\Delta t|z)P(z,t|x), \tag{A3}$$

where the integration is over all possible values the Markov process may access.

Now we consider the time rate of change of $P(y,t|x)$. For an infinitesimal Δt, we can write, by definition,

$$\frac{\partial}{\partial t}P(y,t|x)=\lim_{\Delta t\to 0}\frac{1}{\Delta t}\left[P(y,t+\Delta t|x)-P(y,t|x)\right] \tag{A4}$$

$$=\lim_{\Delta t\to 0}\frac{1}{\Delta t}\left[\int \mathrm{d}z P(y,\Delta t|z)P(z,t|x)-\int \mathrm{d}z P(z,\Delta t|y)P(y,t|x)\right] \tag{A5}$$

$$=\int \mathrm{d}z\left[\lim_{\Delta t\to 0}\frac{P(y,\Delta t|z)}{\Delta t}P(z,t|x)-\lim_{\Delta t\to 0}\frac{P(z,\Delta t|y)}{\Delta t}P(y,t|x)\right], \tag{A6}$$

where in equation (A5) we have used the Chapman-Kolmogorov equation (A3) and the property (A2). Denoting the transition rate as

$$Q(y|x)=\lim_{\Delta t\to 0}\frac{P(y,\Delta t|x)}{\Delta t}, \tag{A7}$$

which is the transition probability density from x to y per infinitesimal time, equation (A6) thus becomes the master equation that describes time evolution of $P(y,t|x)$ for a general Markov process:

$$\frac{\partial}{\partial t}P(y,t|x)=\int \mathrm{d}z\left[Q(y|z)P(z,t|x)-Q(z|y)P(y,t|x)\right]. \tag{A8}$$

After integration, the first term on the right-hand side gives the probability of entering $(y, y+\mathrm{d}y)$, and the second term the probability of leaving that interval, per infinitesimal time.

For practical calculations, the integral in the master equation is often developed into a series. For this purpose, we integrate on both sides of equation (A4) an arbitrary function $R(y)$, which goes to 0 for $y\to\pm\infty$ sufficiently fast. Using again the Chapman-Kolmogorov equation (A3), we have

$$\int \mathrm{d}y R(y)\frac{\partial}{\partial t}P(y,t|x)=\lim_{\Delta t\to 0}\frac{1}{\Delta t}\left[\int \mathrm{d}y R(y)\int \mathrm{d}z P(y,\Delta t|z)P(z,t|x)-\int \mathrm{d}z R(z)P(z,t|x)\right]. \tag{A9}$$

In the double integral, interchanging the order of integration and expanding $R(y)$ in a Taylor series of $(y-z)$, one gets

$$\int \mathrm{d}y R(y)\frac{\partial}{\partial t}P(y,t|x)=\lim_{\Delta t\to 0}\frac{1}{\Delta t}\sum_{n=1}^{\infty}\frac{1}{n!}\int \mathrm{d}z P(z,t|x)\frac{\mathrm{d}^n R(z)}{\mathrm{d}z^n}\int \mathrm{d}y (y-z)^n P(y,\Delta t|z), \tag{A10}$$

in which the integral over y on the right-hand side is the nth statistical moment and its quotient with infinitesimal time gives the nth transport coefficient (apart from a factor of $1/n!$)

$$\alpha_n(z)=\lim_{\Delta t\to 0}\frac{1}{\Delta t}\int dy (y-z)^n P(y,\Delta t|z). \tag{A11}$$

Integrating over z by parts in equation (A10) and then writing y for z yields

$$\int \mathrm{d}y R(y)\frac{\partial}{\partial t}P(y,t|x)=\int \mathrm{d}y R(y)\sum_{n=1}^{\infty}\frac{(-1)^n}{n!}\frac{\partial^n}{\partial y^n}\left[\alpha_n(y)P(y,t|x)\right]. \tag{A12}$$

Finally, since this equation must hold for arbitrary $R(y)$, we are left with the Kramers-Moyal expansion (Kramers, 1940; Moyal, 1949) of the master equation

$$\frac{\partial}{\partial t}P(y,t|x)=\sum_{n=1}^{\infty}\frac{(-1)^n}{n!}\frac{\partial^n}{\partial y^n}\left[\alpha_n(y)P(y,t|x)\right]. \tag{A13}$$

The Kramers-Moyal expansion is a converging series when, in small times, the value of the Markov process can only change with small amounts, or more precisely, when only the first n' statistical moments are proportional to Δt, thus surviving the limit $\Delta t \to 0$ in equation (A11), and all higher moments are of higher orders in Δt. In the case that $n' = 2$, the expansion gives the Fokker-Planck equation

$$\frac{\partial}{\partial t}P(y,t|x) = -\frac{\partial}{\partial y}\left[\alpha_1(y)P(y,t|x)\right] + \frac{1}{2}\frac{\partial^2}{\partial y^2}\left[\alpha_2(y)P(y,t|x)\right]. \tag{A14}$$

As a final remark, since the distribution function (probability density function) of a Markov process can be obtained by convolving $P(y,t|x,0)$ with a given initial distribution, the equations satisfied by the transition probability density in this appendix are therefore also satisfied by the distribution function.

Acknowledgments
This work was supported by NASA grants 80NSSC18K1224 and NNX15AF55G and AFOSR grant FA9550-16-1-0344. Simulation data are accessible at repository (http://doi.org/10.5281/zenodo.2634708).

References

Albert, J. M. (2000). Gyroresonant interactions of radiation belt particles with a monochromatic electromagnetic wave. *Journal of Geophysical Research*, *105*(A9), 21,191–21,209. https://doi.org/10.1029/2000JA000008

Albert, J. M. (2002). Nonlinear interaction of outer zone electrons with VLF waves. *Geophysical Research Letters*, *29*(8), 1275. https://doi.org/10.1029/2001GL013941

Albert, J. M., & Bortnik, J. (2009). Nonlinear interaction of radiation belt electrons with electromagnetic ion cyclotron waves. *Geophysical Research Letters*, *36*, L12110. https://doi.org/10.1029/2009GL038904

Albert, J. M., Tao, X., & Bortnik, J. (2013). Aspects of nonlinear wave-particle interactions. In *Dynamics of the Earth's radiation belts and inner magnetosphere* (pp. 255–264). Washington, DC: American Geophysical Union. https://doi.org/10.1029/2012GM001324

Ames, W. F. (2014). *Numerical methods for partial differential equations*. Verlag London: Academic Press.

Anderson, B. J., Erlandson, R. E., & Zanetti, L. J. (1992). A statistical study of Pc 1–2 magnetic pulsations in the equatorial magnetosphere: 1. Equatorial occurrence distributions. *Journal of Geophysical Research*, *97*(A3), 3075–3088. https://doi.org/10.1029/91JA02706

Artemyev, A., Krasnoselskikh, V., Agapitov, O., Mourenas, D., & Rolland, G. (2012). Non-diffusive resonant acceleration of electrons in the radiation belts. *Plasma Physics*, *19*(12), 122901. https://doi.org/10.1063/1.4769726

Artemyev, A., Neishtadt, A., Vainchtein, D., Vasiliev, A., Vasko, I., & Zelenyi, L. (2018). Trapping (capture) into resonance and scattering on resonance: Summary of results for space plasma systems. *Communications in Nonlinear Science and Numerical Simulation*, *65*, 111–160. https://doi.org/10.1016/j.cnsns.2018.05.004

Artemyev, A. V., Neishtadt, A. I., Vasiliev, A. A., & Mourenas, D. (2016). Kinetic equation for nonlinear resonant wave-particle interaction. *Physics of Plasmas*, *23*(9), 090701. https://doi.org/10.1063/1.4962526

Artemyev, A. V., Neishtadt, A. I., Vasiliev, A. A., & Mourenas, D. (2017). Probabilistic approach to nonlinear wave-particle resonant interaction. *Physical Review E*, *95*, 023204. https://doi.org/10.1103/PhysRevE.95.023204

Artemyev, A. V., Neishtadt, A. I., Vasiliev, A. A., & Mourenas, D. (2018). Long-term evolution of electron distribution function due to nonlinear resonant interaction with whistler mode waves. *Journal of Plasma Physics*, *84*(2), 905840206. https://doi.org/10.1017/S0022377818000260

Bortnik, J., Thorne, R. M., & Meredith, N. P. (2008). The unexpected origin of plasmaspheric hiss from discrete chorus emissions. *Nature*, *452*, 62–66. https://doi.org/10.1038/nature06741

Chandrasekhar, S. (1943). Stochastic problems in physics and astronomy. *Reviews of Modern Physics*, *15*, 1–89. https://doi.org/10.1103/RevModPhys.15.1

Chang, H. C., & Inan, U. S. (1983). Quasi-relativistic electron precipitation due to interactions with coherent VLF waves in the magnetosphere. *Journal of Geophysical Research*, *88*(A1), 318–328. https://doi.org/10.1029/JA088iA01p00318

Chen, L., Thorne, R. M., Bortnik, J., & Zhang, X.-J. (2016). Nonresonant interactions of electromagnetic ion cyclotron waves with relativistic electrons. *Journal of Geophysical Research: Space Physics*, *121*, 9913–9925. https://doi.org/10.1002/2016JA022813

Chen, L., Thorne, R. M., Jordanova, V. K., Wang, C.-P., Gkioulidou, M., Lyons, L., & Horne, R. B. (2010). Global simulation of EMIC wave excitation during the 21 April 2001 storm from coupled RCM-RAM-HOTRAY modeling. *Journal of Geophysical Research*, *115*, A07209. https://doi.org/10.1029/2009JA015075

Davidson, G. T. (1976). An improved empirical description of the bounce motion of trapped particles. *Journal of Geophysical Research*, *81*(22), 4029–4030. https://doi.org/10.1029/JA081i022p04029

Doob, J. L. (1953). *Stochastic processes*. New York: Wiley.

Fennell, J. F., Roeder, J. L., Kurth, W. S., Henderson, M. G., Larsen, B. A., Hospodarsky, G., et al. (2014). Van Allen Probes observations of direct wave-particle interactions. *Geophysical Research Letters*, *41*, 1869–1875. https://doi.org/10.1002/2013GL059165

Fraser, B. J., Grew, R. S., Morley, S. K., Green, J. C., Singer, H. J., Loto'aniu, T. M., & Thomsen, M. F. (2010). Storm time observations of electromagnetic ion cyclotron waves at geosynchronous orbit: GOES results. *Journal of Geophysical Research*, *115*, A05208. https://doi.org/10.1029/2009JA014516

Fraser, B. J., Singer, H. J., Hughes, W. J., Wygant, J. R., Anderson, R. R., & Hu, Y. D. (1996). CRRES Poynting vector observations of electromagnetic ion cyclotron waves near the plasmapause. *Journal of Geophysical Research*, *101*(A7), 15,331–15,343. https://doi.org/10.1029/95JA03480

Furuya, N., Omura, Y., & Summers, D. (2008). Relativistic turning acceleration of radiation belt electrons by whistler mode chorus. *Journal of Geophysical Research*, *113*, A04224. https://doi.org/10.1029/2007JA012478

Glauert, S. A., & Horne, R. B. (2005). Calculation of pitch angle and energy diffusion coefficients with the PADIE code. *Journal of Geophysical Research*, *110*, A04206. https://doi.org/10.1029/2004JA010851

Horne, R. B., & Thorne, R. M. (1993). On the preferred source location for the convective amplification of ion cyclotron waves. *Journal of Geophysical Research*, *98*(A6), 9233–9247. https://doi.org/10.1029/92JA02972

Horne, R. B., & Thorne, R. M. (1994). Convective instabilities of electromagnetic ion cyclotron waves in the outer magnetosphere. *Journal of Geophysical Research*, *99*(A9), 17,259–17,273. https://doi.org/10.1029/94JA01259

Inan, U. S., Bell, T. F., & Helliwell, R. A. (1978). Nonlinear pitch angle scattering of energetic electrons by coherent VLF waves in the magnetosphere. *Journal of Geophysical Research*, *83*(A7), 3235–3253. https://doi.org/10.1029/JA083iA07p03235

Jordanova, V. K., Albert, J., & Miyoshi, Y. (2008). Relativistic electron precipitation by EMIC waves from self-consistent global simulations. *Journal of Geophysical Research*, *113*, A00A10. https://doi.org/10.1029/2008JA013239

Jordanova, V. K., Farrugia, C. J., Thorne, R. M., Khazanov, G. V., Reeves, G. D., & Thomsen, M. F. (2001). Modeling ring current proton precipitation by electromagnetic ion cyclotron waves during the May 14–16, 1997, storm. *Journal of Geophysical Research*, *106*(A1), 7–22. https://doi.org/10.1029/2000JA002008

Jordanova, V. K., Miyoshi, Y. S., Zaharia, S., Thomsen, M. F., Reeves, G. D., Evans, D. S., et al. (2006). Kinetic simulations of ring current evolution during the Geospace Environment Modeling challenge events. *Journal of Geophysical Research*, *111*, A11S10. https://doi.org/10.1029/2006JA011644

Kennel, C. F., & Engelmann, F. (1966). Velocity space diffusion from weak plasma turbulence in a magnetic field. *Physics of Fluids*, *9*(12), 2377–2388. https://doi.org/10.1063/1.1761629

Kozyra, J. U., Cravens, T. E., Nagy, A. F., Fontheim, E. G., & Ong, R. S. B. (1984). Effects of energetic heavy ions on electromagnetic ion cyclotron wave generation in the plasmapause region. *Journal of Geophysical Research*, *89*(A4), 2217–2233. https://doi.org/10.1029/JA089iA04p02217

Kramers, H. A. (1940). Brownian motion in a field of force and the diffusion model of chemical reactions. *Physica*, *7*(4), 284–304. https://doi.org/10.1016/S0031-8914(40)90098-2

Li, J., Bortnik, J., Xie, L., Pu, Z., Chen, L., Ni, B., et al. (2015). Comparison of formulas for resonant interactions between energetic electrons and oblique whistler-mode waves. *Plasma Physics*, *22*(5), 052902. https://doi.org/10.1063/1.4914852

Li, Z., Millan, R. M., & Hudson, M. K. (2013). Simulation of the energy distribution of relativistic electron precipitation caused by quasi-linear interactions with EMIC waves. *Journal of Geophysical Research: Space Physics*, *118*, 7576–7583. https://doi.org/10.1002/2013JA019163

Liu, K., Lemons, D. S., Winske, D., & Gary, S. P. (2010). Relativistic electron scattering by electromagnetic ion cyclotron fluctuations: Test particle simulations. *Journal of Geophysical Research*, *115*, A04204. https://doi.org/10.1029/2009JA014807

Liu, K., Winske, D., Gary, S. P., & Reeves, G. D. (2012). Relativistic electron scattering by large amplitude electromagnetic ion cyclotron waves: The role of phase bunching and trapping. *Journal of Geophysical Research*, *117*, A06218. https://doi.org/10.1029/2011JA017476

Lyons, L. R. (1974). Pitch angle and energy diffusion coefficients from resonant interactions with ion-cyclotron and whistler waves. *Journal of Plasma Physics*, *12*, 417–432. https://doi.org/10.1017/S002237780002537X

Lyons, L. R., & Williams, D. J. (1984). *Quantitative aspects of magnetospheric physics*. Norwell, MA: D. Reidel.

Maldonado, A. A., & Chen, L. (2018). On the diffusion rates of electron bounce resonant scattering by magnetosonic waves. *Geophysical Research Letters*, *45*, 3328–3337. https://doi.org/10.1002/2017GL076560

Marshall, R. A., & Bortnik, J. (2018). Pitch angle dependence of energetic electron precipitation: Energy deposition, backscatter, and the bounce loss cone. *Journal of Geophysical Research: Space Physics*, *123*, 2412–2423. https://doi.org/10.1002/2017JA024873

Mauk, B. H., & McPherron, R. L. (1980). An experimental test of the electromagnetic ion cyclotron instability within the Earth's magnetosphere. *Physics of Fluids*, *23*(10), 2111–2127. https://doi.org/10.1063/1.862873

Meredith, N. P., Thorne, R. M., Horne, R. B., Summers, D., Fraser, B. J., & Anderson, R. R. (2003). Statistical analysis of relativistic electron energies for cyclotron resonance with EMIC waves observed on CRRES. *Journal of Geophysical Research*, *108*(A6), 1250. https://doi.org/10.1029/2002JA009700

Miyoshi, Y., Sakaguchi, K., Shiokawa, K., Evans, D., Albert, J., Connors, M., & Jordanova, V. (2008). Precipitation of radiation belt electrons by EMIC waves, observed from ground and space. *Geophysical Research Letters*, *35*, L23101. https://doi.org/10.1029/2008GL035727

Morley, S. K., Ables, S. T., Sciffer, M. D., & Fraser, B. J. (2009). Multipoint observations of Pc1–2 waves in the afternoon sector. *Journal of Geophysical Research*, *114*, A09205. https://doi.org/10.1029/2009JA014162

Moyal, J. E. (1949). Stochastic processes and statistical physics. *Journal of the Royal Statistical Society. Series B*, *11*(2), 150–210.

Omura, Y., Katoh, Y., & Summers, D. (2008). Theory and simulation of the generation of whistler-mode chorus. *Journal of Geophysical Research*, *113*, A04223. https://doi.org/10.1029/2007JA012622

Omura, Y., Miyashita, Y., Yoshikawa, M., Summers, D., Hikishima, M., Ebihara, Y., & Kubota, Y. (2015). Formation process of relativistic electron flux through interaction with chorus emissions in the Earth's inner magnetosphere. *Journal of Geophysical Research: Space Physics*, *120*, 9545–9562. https://doi.org/10.1002/2015JA021563

Omura, Y., & Summers, D. (2004). Computer simulations of relativistic whistler-mode wave-particle interactions. *Physics of Plasmas*, *11*(7), 3530–3534. https://doi.org/10.1063/1.1757457

Reif, F. (1965). *Fundamentals of statistical and thermal physics*. New York: McGraw-Hill.

Schulz, M., & Lanzerotti, L. J. (1974). *Particle diffusion in the radiation belts*. New York: Springer-Verlag.

Shprits, Y. Y. (2009). Potential waves for pitch-angle scattering of near-equatorially mirroring energetic electrons due to the violation of the second adiabatic invariant. *Geophysical Research Letters*, *36*, L12106. https://doi.org/10.1029/2009GL038322

Shprits, Y. Y., Drozdov, A. Y., Spasojevic, M., Kellerman, A. C., Usanova, M. E., Engebretson, M. J., et al. (2016). Wave-induced loss of ultra-relativistic electrons in the Van Allen radiation belts. *Nature Communications*, *7*, 12883. https://doi.org/10.1038/ncomms12883

Stix, T. H. (1962). *The theory of plasma waves*. New York: McGraw Hill.

Su, Z., Zhu, H., Xiao, F., Zheng, H., Shen, C., Wang, Y., & Wang, S. (2012). Bounce-averaged advection and diffusion coefficients for monochromatic electromagnetic ion cyclotron wave: Comparison between test-particle and quasi-linear models. *Journal of Geophysical Research*, *117*, A09222. https://doi.org/10.1029/2012JA017917

Summers, D., & Thorne, R. M. (2003). Relativistic electron pitch-angle scattering by electromagnetic ion cyclotron waves during geomagnetic storms. *Journal of Geophysical Research*, *108*(A4), 1143. https://doi.org/10.1029/2002JA009489

Tao, X., & Bortnik, J. (2010). Nonlinear interactions between relativistic radiation belt electrons and oblique whistler mode waves. *Nonlinear Processes in Geophysics*, *17*(5), 599.

Tao, X., Bortnik, J., Albert, J., Liu, K., & Thorne, R. (2011). Comparison of quasi-linear diffusion coefficients for parallel propagating whistler mode waves with test particle simulations. *Geophysical Research Letters*, *38*, L06105. https://doi.org/10.1029/2011GL046787

Tao, X., Bortnik, J., Thorne, R. M., Albert, J. M., & Li, W. (2012). Effects of amplitude modulation on nonlinear interactions between electrons and chorus waves. *Geophysical Research Letters*, *39*, L06102. https://doi.org/10.1029/2012GL051202

Thorne, R. M., & Horne, R. B. (1997). Modulation of electromagnetic ion cyclotron instability due to interaction with ring current O^+ during magnetic storms. *Journal of Geophysical Research*, *102*(A7), 14,155–14,163. https://doi.org/10.1029/96JA04019

Thorne, R. M., & Kennel, C. F. (1971). Relativistic electron precipitations during magnetic storm main phase. *Journal of Geophysical Research*, *76*, 4446–4453. https://doi.org/10.1029/JA076i019p04446

Wang, M. C., & Uhlenbeck, G. E. (1945). On the theory of the Brownian motion II. *Reviews of Modern Physics*, *17*(2-3), 323–342. https://doi.org/10.1103/RevModPhys.17.323

Woodger, L. A., Halford, A. J., Millan, R. M., McCarthy, M. P., Smith, D. M., Bowers, G. S., et al. (2015). A summary of the BARREL campaigns: Technique for studying electron precipitation. *Journal of Geophysical Research: Space Physics*, *120*, 4922–4935. https://doi.org/10.1002/2014JA020874

Zank, G. P. (2014). *Transport processes in space physics and astrophysics*. Switzerland: Springer. https://doi.org/10.1007/978-1-4614-8480-6